

ARMY RESEARCH LABORATORY



# Dynamic Consolidation of Combustion Synthesized Alumina-Titanium Diboride Ceramic Composites

Laszlo J. Kecskes  
Andrus Niiler  
Thomas Kottke  
U.S. ARMY RESEARCH LABORATORY

Kathryn V. Logan  
Guillermo R. Villalobos  
GEORGIA INSTITUTE OF TECHNOLOGY

ARL-TR-918

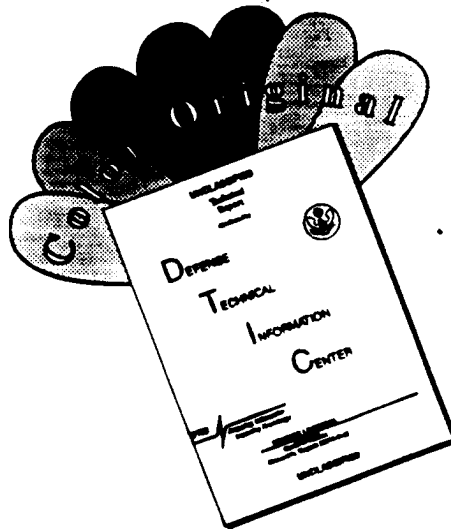
December 1995

19960206 022

APPROVED FOR PUBLIC RELEASE; DISTRIBUTION IS UNLIMITED.

DTIC QUALITY INSPECTED 1

# DISCLAIMER NOTICE



THIS DOCUMENT IS BEST QUALITY AVAILABLE. THE COPY FURNISHED TO DTIC CONTAINED A SIGNIFICANT NUMBER OF COLOR PAGES WHICH DO NOT REPRODUCE LEGIBLY ON BLACK AND WHITE MICROFICHE.

## **NOTICES**

Destroy this report when it is no longer needed. DO NOT return it to the originator.

Additional copies of this report may be obtained from the National Technical Information Service, U.S. Department of Commerce, 5285 Port Royal Road, Springfield, VA 22161.

The findings of this report are not to be construed as an official Department of the Army position, unless so designated by other authorized documents.

The use of trade names or manufacturers' names in this report does not constitute indorsement of any commercial product.

# REPORT DOCUMENTATION PAGE

Form Approved  
OMB No. 0704-0188

Public reporting burden for this collection of information is estimated to average 1 hour per response, including the time for reviewing instructions, searching existing data sources, gathering and maintaining the data needed, and completing and reviewing the collection of information. Send comments regarding this burden estimate or any other aspect of this collection of information, including suggestions for reducing this burden, to Washington Headquarters Services, Directorate for Information Operations and Reports, 1215 Jefferson Davis Highway, Suite 1204, Arlington, VA 22202-4302, and to the Office of Management and Budget, Paperwork Reduction Project (0704-0188), Washington, DC 20503.

1. AGENCY USE ONLY (Leave blank)		2. REPORT DATE December 1995		3. REPORT TYPE AND DATES COVERED Final, 1 Oct 1989-1 Oct 1991	
4. TITLE AND SUBTITLE Dynamic Consolidation of Combustion Synthesized Alumina-Titanium Diboride Ceramic Composites				5. FUNDING NUMBERS PR: 1L161102AH43 WO: 61102A	
6. AUTHOR(S) L. J. Kecskes, A. Niiler, T. Kottke (ARL), K. V. Logan, and G. R. Villalobos (GTRI)					
7. PERFORMING ORGANIZATION NAME(S) AND ADDRESS(ES) U.S. Army Research Laboratory ATTN: AMSRL-WT-WD Aberdeen Proving Ground, MD 21005-5066 Georgia Tech Research Institute Georgia Institute of Technology Dalney St., Baker Bldg. Atlanta, GA 30332				8. PERFORMING ORGANIZATION REPORT NUMBER ARL-TR-918	
9. SPONSORING / MONITORING AGENCY NAME(S) AND ADDRESS(ES)				10. SPONSORING / MONITORING AGENCY REPORT NUMBER	
11. SUPPLEMENTARY NOTES					
12a. DISTRIBUTION / AVAILABILITY STATEMENT Approved for public release; distribution is unlimited.				12b. DISTRIBUTION CODE	
13. ABSTRACT (Maximum 200 words) A mixture of $TiO_2$ , $B_2O_3$ , and Al powders was reacted exothermically to form a low-density $Al_2O_3$ -TiB <sub>2</sub> foamed product. After the cessation of the combustion synthesis reaction, this hot foam was densified by the pressure waves generated by the detonation of an explosive charge. The delay time between the initiation of the combustion synthesis and detonation of the explosive, the thickness of the explosive charge, and the strength of sample confinement were found to influence the effectiveness of the consolidation. Analysis of the combustion synthesis reaction temperature histories and microscopy of the reacted product sponge are used to develop additional information about this reaction/consolidation process. These results, and the microstructural properties of the combustion-synthesized and dynamically consolidated products, are discussed.					
14. SUBJECT TERMS alumina, titanium diboride, ceramic-ceramic composite, combustion synthesis, SHS, dynamic consolidation, explosive compaction, microstructure, processing, powdered precursors, properties				15. NUMBER OF PAGES 35	
				16. PRICE CODE	
17. SECURITY CLASSIFICATION OF REPORT UNCLASSIFIED	18. SECURITY CLASSIFICATION OF THIS PAGE UNCLASSIFIED	19. SECURITY CLASSIFICATION OF ABSTRACT UNCLASSIFIED	20. LIMITATION OF ABSTRACT UL		

INTENTIONALLY LEFT BLANK.

## ACKNOWLEDGMENTS

We wish to thank Mr. Frederick B. Pierce of the Weapons Technology Directorate for his extensive contributions to these experiments, and summer student Ms. Sharon H. Robinson for the microhardness measurements and metallographic preparation of the samples. Additionally, we appreciate Messrs. Ralph F. Benck and Paul H. Netherwood, Jr., for their highly valuable suggestions during the experiments, as well as the thorough reading and critique of this manuscript.

INTENTIONALLY LEFT BLANK.

## TABLE OF CONTENTS

	<u>Page</u>
ACKNOWLEDGMENTS .....	iii
LIST OF FIGURES .....	vii
LIST OF TABLES .....	ix
1. INTRODUCTION .....	1
2. EXPERIMENTAL PROCEDURE .....	3
3. RESULTS AND DISCUSSION .....	8
3.1 Auxiliary Temperature Measurement .....	8
3.2 CS/DC Experiments .....	13
4. CONCLUSIONS .....	26
5. REFERENCES .....	27
DISTRIBUTION LIST .....	31

INTENTIONALLY LEFT BLANK.

## LIST OF FIGURES

<u>Figure</u>	<u>Page</u>
1. Backscattered electron micrograph of the precursor powder mixture in 1A, Al EDS dot map in 1B, and Ti EDS dot map in 1C .....	4
2. Schematic arrangement of the thermocouples and pyrometers in the temperature-time measurement .....	6
3. Diagrammatic representation of the $\text{Al}_2\text{O}_3$ - $\text{TiB}_2$ reaction process .....	9
4. Temperature data for the $\text{Al}_2\text{O}_3$ - $\text{TiB}_2$ system. Thermocouple data are shown in 4A, and pyrometer data are shown in 4B .....	10
5. Macrograph of the reacted, but uncompact sample in 5A, with enlargements of typical microstructural features in 5B and 5C .....	12
6. Typical CS/DC $\text{Al}_2\text{O}_3$ - $\text{TiB}_2$ sample with top and bottom views shown in 6A and 6B, respectively .....	14
7. $\text{Al}_2\text{O}_3$ - $\text{TiB}_2$ sample density vs. delay time .....	17
8. Optical macrophotographs of polished cross sections of the samples with a $t_d$ of 4.2 s in 8A, 11.4 s in 8B, 12.1 s in 8C, 16.8 s in 8D, 38.9 s in 8E, and 58.8 s in 8F .....	18
9. Backscattered electron micrographs of the $\text{Al}_2\text{O}_3$ - $\text{TiB}_2$ samples with a $t_d$ of 4.2 s in 9A, 11.4 s in 9B, 12.1 s in 9C, 16.8 s in 9D, 38.9 s in 9E, and 58.8 s in 9F .....	19
10. Degree of aggregation and intermixing of the $\text{Al}_2\text{O}_3$ and $\text{TiB}_2$ phases in the S60 (38.9 s) sample. The central region is shown in 10A, and the edge region is shown in 10B .....	21
11. Characteristic fracture surfaces of the $\text{Al}_2\text{O}_3$ - $\text{TiB}_2$ samples. The S59 (4.2 s) sample shown in 11A, the S57 (11.4 s) sample in 11B, and the S60 (38.9 s) sample in 11C .....	22
12. Inhomogeneity of the $\text{Al}_2\text{O}_3$ - $\text{TiB}_2$ samples. External contamination is shown in 12A, and incomplete conversion of reactants to products is shown in 12B .	25

INTENTIONALLY LEFT BLANK.

## LIST OF TABLES

<u>Table</u>	<u>Page</u>
1. $\text{Al}_2\text{O}_3\text{-TiB}_2$ Sample Density and Microhardness . . . . .	15
2. X-ray Diffraction Results of $\text{Al}_2\text{O}_3\text{-TiB}_2$ Samples . . . . .	16

INTENTIONALLY LEFT BLANK.

## 1. INTRODUCTION

Ceramic-ceramic composites that successfully combine the advantageous properties of the individual components are of special interest to the ceramic industry. For example, when TiC or TiB<sub>2</sub> is combined with Al<sub>2</sub>O<sub>3</sub>, the composite, without a significant drop in overall microhardness, has better oxidation resistance (Matsushita, Hayashi, and Saito 1990; Tampieri, Landi, and Bellosi 1992; Cutler, Hurford, and Virkar, 1989; Ishigaki, Sato, and Moriyoshi 1989) and possesses superior mechanical strength (Kimura et al. 1989; Stadlbauer, Kladnig, and Gritzner 1989; Vershinnikov, Mamyran, and Georgiev 1993) and fracture toughness (Furukawa, Nakano, and Takashuna 1988) than TiC or TiB<sub>2</sub> alone. Typically, such ceramic materials are fabricated into monolithic structures by consolidating mixed precursor ceramic powders by either hot-pressing or hot-isostatic-pressing operations. Since the Al<sub>2</sub>O<sub>3</sub>-TiC and Al<sub>2</sub>O<sub>3</sub>-TiB<sub>2</sub> systems readily lend themselves to fabrication via combustion synthesis, both composites can be directly manufactured from their elemental and oxide/boride precursors. The focus of this report is the ceramic system that forms during the simultaneous reduction of the oxides of titanium and boron by aluminum.

Combustion-synthesis processing (also known as self-propagating high-temperature, SHS, or reaction synthesis) has been used extensively during the past three decades to form a wide spectrum of ceramic materials (Merzhanov 1990; Materials Research Society 1993; Metals Powder Industries Federation 1992; TMS 1992; Munir and Holt 1990). Generally, these ceramics are highly sensitive to minute levels of contaminants on the precursors, and, due to physical, thermodynamic, and kinetic factors associated with the process, the products usually contain high levels of porosity and exhibit extensive cracking. Consequently, the combustion-synthesized ceramics require some form of externally applied pressure to achieve complete densification. Reviews of the combustion synthesis process, its historical development, and basic characteristics can be found in McCauley (1990), Munir and Anselmi-Tamburini (1989), and Munir (1988).

The inherent porosity (sometimes as much as 50%) can be reduced if the reacted ceramic product is consolidated while it is at a temperature above the ductile-brittle transition temperature

or, in some cases, the melting point of the material. This densification step could be accomplished by a variety of conventional (slow) powder metallurgy methods such as hot-pressing or hot-isostatic-pressing or, alternatively, by more rapid techniques using high-pressure gases (Miyamoto, Koizumi, and Yamada 1984; Yamada, Miyamoto, and Koizumi 1987; Adachi et al. 1989; Nishida et al. 1993), hot-rolling (Rice et al. 1986), high-speed forges/presses (Hoke et al. 1992; Vecchio et al. 1992; LaSalvia, Meyer, and Meyers 1992; Misiolek, Schurman, and Sopchak 1992), or explosives (Niiler et al. 1988; Niiler, Kecskes, and Kottke 1990; Rabin, Korth, and Williamson 1990; Grebe et al. 1992; Wang, Wixom, and Thompson 1994).

The combustion synthesis dynamic consolidation (CS/DC) method for producing monolithic, full-density TiC and TiB<sub>2</sub> has been developed at the U.S. Army Research Laboratory (ARL), formerly the Ballistic Research Laboratory (Niiler et al. 1988; Niiler, Kecskes, and Kottke 1990). This technique where the two independent processes of CS and DC are effectively combined has been subsequently adapted to other binary ceramic systems (Kecskes, Benck, and Netherwood 1990). The relevant aspects of the CS/DC method and those of the resultant ceramics can be found elsewhere (Kecskes, Niiler, and Kottke 1990, 1993). To date, limited efforts have extended the applicability of this technique to more complex combustion synthesis systems such as TiC-TiB<sub>2</sub> (Kecskes et al. 1990; Kecskes, Kottke, and Puszynski, to be published) and TiC-Al<sub>2</sub>O<sub>3</sub> (Rabin, Korth, and Williamson 1990).

The primary objective of this effort was to demonstrate that, with slight modifications, the CS/DC technique developed for combustion-synthesized TiC, TiB<sub>2</sub>, and HfC can also be adapted to heterogeneous ceramic composite systems. The secondary objective was to identify the necessary modifications and determine the effects, on the fabricated Al<sub>2</sub>O<sub>3</sub>-TiB<sub>2</sub>, of the various experimental conditions that were required for the successful reaction and consolidation of TiC and TiB<sub>2</sub>. Specifically, the effects of sample configuration, sample confinement, reaction ignition-consolidation delay time (referred to as delay time hereafter), and explosive loading in the reaction/consolidation system were evaluated. The key features of the process, as well as some of the characteristics and properties of the Al<sub>2</sub>O<sub>3</sub>-TiB<sub>2</sub> ceramics produced, are described.

## 2. EXPERIMENTAL PROCEDURE

The ARL reaction/consolidation assembly consists of two distinct components, the reaction fixture and the explosive driver package. The reaction fixture encompasses a thin-walled steel ring surrounded by a porous gypsum,  $\text{CaSO}_4 \times 2\text{H}_2\text{O}$ , (wallboard) container. This configuration allows the reaction to take place, maintains the reacted product at an elevated temperature, and serves as a crushable medium during consolidation. The explosive driver package consists of two high-hardness steel compression plates (Brinell Hardness of 480–530) and a suitable container for the powdered amatol explosive (80/20  $\text{NH}_4\text{NO}_3/\text{TNT}$ ) and functions to provide the high pressures needed to densify the reaction product.

The precursor powders consisted of high-purity, 99.7%, 15- to 19- $\mu\text{m}$ , (Fisher sizing) grade 123, aluminum (Al) metal powder (ALCOA, Pittsburgh, PA), min. 98.5% purity, –250- $\mu\text{m}$  (–60 Mesh) (Stock No. A76-500), reagent-grade boron trioxide ( $\text{B}_2\text{O}_3$ ) (Fisher Chemicals, Pittsburgh, PA), and 99.0% purity, 0.3- $\mu\text{m}$  (Stock No. T315-500), reagent-grade titanium dioxide ( $\text{TiO}_2$ ) (Fisher Chemicals, Pittsburgh, PA). These powders were thoroughly dry-mixed under argon in an atomic ratio of 10:3:3 ( $\text{Al}:\text{B}_2\text{O}_3:\text{TiO}_2$ ). A cursory examination of the powders with scanning electron microscopy (SEM) (JEOL, Peabody, MA) and energy dispersive x-ray spectroscopy (EDS) (Noran Instruments, Middleton, WI) indicated that the powders were within the manufacturers' specifications. A backscattered electron image and Al and Ti EDS dot maps of the precursor powder mixture are shown in Figure 1. Although  $\text{B}_2\text{O}_3$  was also present in the powder mixture, the characteristic boron and oxygen x-ray lines could not be observed due to absorption in the EDS detector window. As verified by the Al and Ti EDS dot maps, the extremely fine  $\text{TiO}_2$  particles tend to adhere and coat the much larger Al particles in the mixture.

The powder mixture was uniaxially pressed at 45 MPa, to form cylindrical green compacts 50.8 mm in diameter with a height of about 25 mm. This green compact was inserted into a steel ring that was lined with a chemically inert Grafoil (Union Carbide, Cleveland, OH) sheet barrier to prevent external contamination of the sample. The compact was further thermally insulated from the steel plates with zirconia felt (Zircar Products, Inc., Florida, NY). An electric

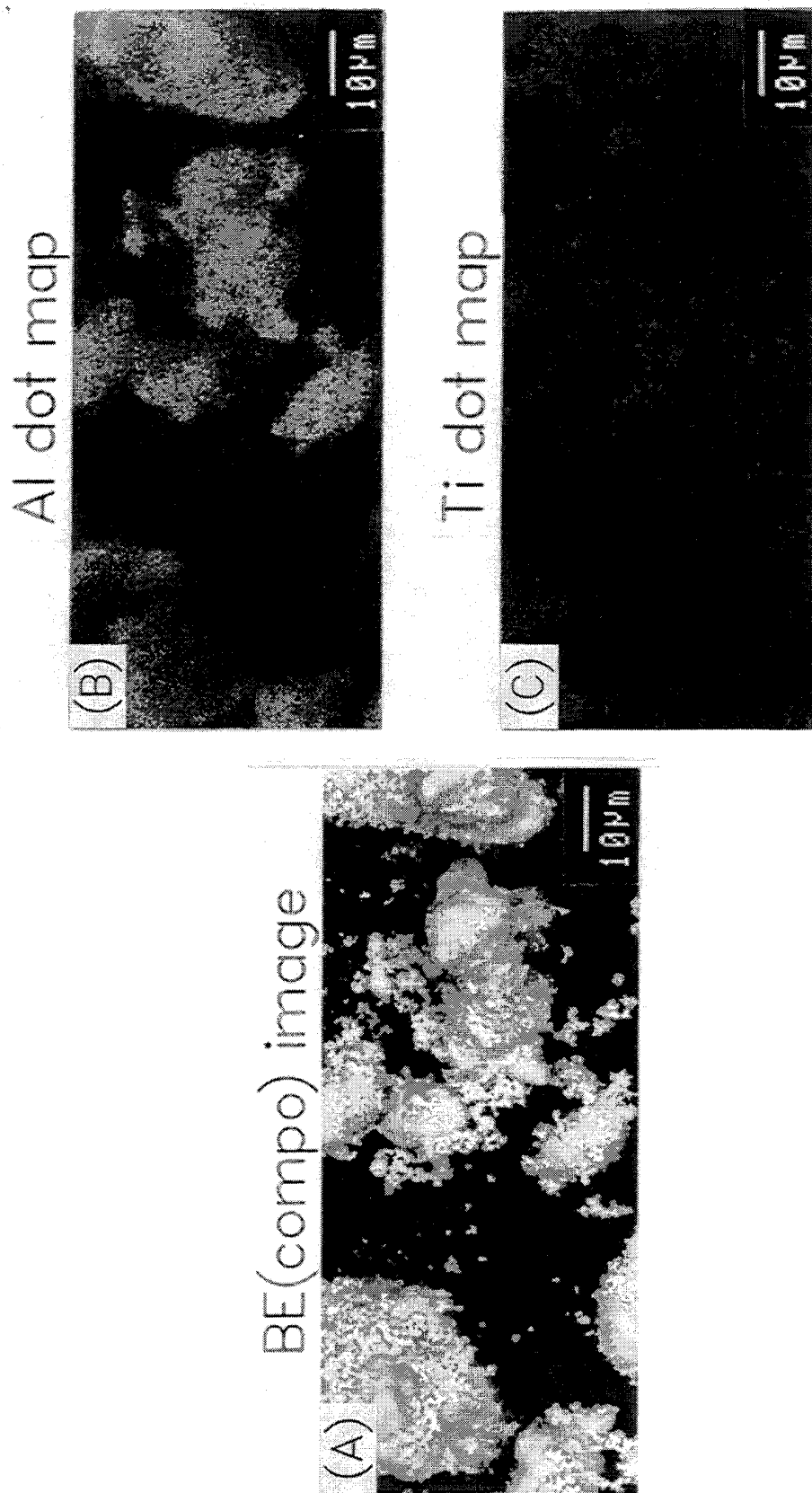


Figure 1. Backscattered electron micrograph of the precursor powder mixture in 1A, Al EDS dot map in 1B, and Ti EDS dot map in 1C.

match was placed at the center of the top of the compact, and a small amount of Ti-B igniter powder mixture was pressed into place around the electric match. The polymethyl methacrylate (PMMA) explosive driver package was loaded with the amatol charge and affixed to the top of the reaction fixture as the final step in the assembly procedure. The majority of the CS/DC experiments were performed with a c:m (explosive charge mass to compression plate mass) ratio of 0.22. A few preliminary experiments were also done with c:m ratios of 0.33 and 0.44.

Prior to firing, the SHS and explosive components were combined, and the reaction/consolidation assembly was placed on top of a 2- to 3-m-high sandpile. The electric match was activated, igniting the igniter mixture, which, in turn, ignited the green compact. The elapsed time between ignition of the CS reaction and the detonation of the explosive charge was varied from 4 to 59 s. The subsequent detonation compacted the hot  $\text{Al}_2\text{O}_3\text{-TiB}_2$  pellet and drove the entire assembly several inches into the sand. The sample was allowed to cool in the sand for about 30–45 min prior to recovery. Detailed accounts of this procedure have been reported elsewhere (Niiler et al. 1988; Niiler, Kecskes, and Kottke 1990).

Following the removal of the steel ring and thermal insulation, the CS/DC ceramic disks were thoroughly cleaned. This ceramic material is conductive and can be cut by Electric Discharge Machining (EDM) (Metals Research Group, Monsey, NY). Each sample was sliced along a diameter. One half was vacuum-impregnated with epoxy and diamond-lapped to a  $1/4\text{-}\mu\text{m}$  finish. The other half was sectioned further for microstructural analysis. A thin wafer was cut with EDM and then mounted and polished for optical, SEM, EDS, and microhardness measurements.

Sample densities were measured using Archimedes' Principle. The room-temperature sample microhardness was determined using a Knoop indenter with 100-g and 400-g test loads. Hardness values are averages of 15 individual measurements. Quoted error bars indicate the limit of error and are given as  $\pm\sigma/n^{1/2}$ , where  $\sigma$  is the standard deviation of the data set and  $n$  is the number of measurements. Additionally, a small portion of the central section was ground into fine powder for x-ray diffraction (XRD) analysis (Philips Electronic Instruments, Mahwah, NJ).

Finally, a fragment was broken off (by impact loading at room temperature) for evaluation of the sample's intergrain bonding and fracture characteristics.

The CS/DC experiments were preceded by an auxiliary experiment, which determined the time interval during which the material remained above its ductile-brittle transition temperature. This information was essential to ascertain whether this new ceramic material system could be successfully compacted and/or consolidated in the reaction/consolidation fixture. The experiment consisted of measurements of temperature and reaction rate of the reacting green compact.

A reaction fixture, identical to that used in the CS/DC experiments, was equipped with Type K (chromel-alumel) thermocouples and high- and low-temperature pyrometers to obtain the reaction velocity and peak temperatures in the fixture. See Figure 2 for a schematic of the arrangement. The pyrometers were aimed at a circumferential point at the axial midline of the compact. Two sets of dual thermocouples were also used for reaction rate measurements. One of these pairs had a thermocouple that was buried in the igniter mixture at the center of the sample's top surface. The other thermocouple of this pair was placed at the compact's edge. The second set of thermocouples was set up in a similar manner under the bottom of the compact (i.e., one at the bottom center of the disk and the other at its edge).

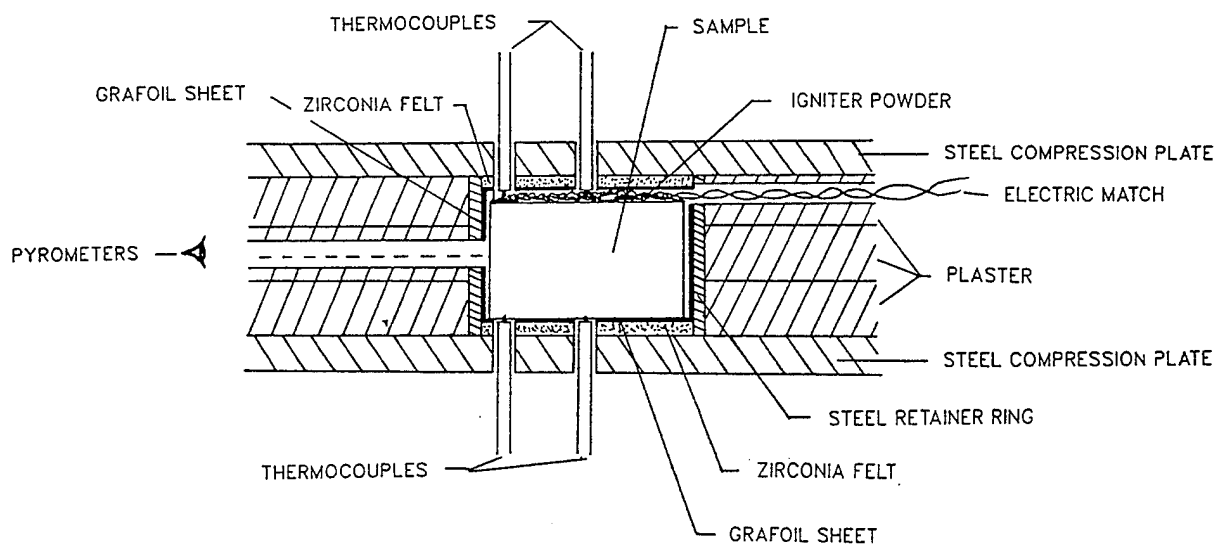
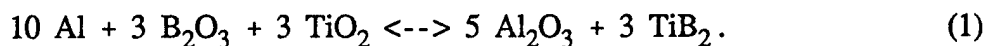


Figure 2. Schematic arrangement of the thermocouples and pyrometers in the temperature-time measurement.

The thermocouple emfs were inputted into a differential voltage amplifier whose output and those of the pyrometers were digitized with a 12-bit D/A converter. The D/A converter was a Metrabyte DAS-16 high-speed analog data acquisition system (Metrabyte Corporation, Taunton, MA). The combustion synthesis reaction was remotely initiated, and the reaction velocity and temperature profile of the reacting green compact were observed in real time on a video display terminal. The data were recorded and stored after the reacted sample cooled to ambient conditions.

### 3. RESULTS AND DISCUSSION

3.1 Auxiliary Temperature Measurement. The reaction mechanism of this three-component system is rather complex and has been extensively studied by Logan and coworkers (Logan, Price, and McLemore 1987; Logan, Sparrow, and McLemore 1990; Logan 1992). Aided with a diagrammatic representation in Figure 3, the following is a brief description, summarizing the rate controlling steps in the reduction of the oxides of boron and titanium by aluminum metal. The overall chemical reaction is given as:



The self-propagating combustion synthesis reaction begins with  $\text{B}_2\text{O}_3$  melting at a low temperature of about  $150^\circ \text{C}$  ( $T_m = 450^\circ \text{C}$ ) and wetting the  $\text{TiO}_2$  and Al particles. With increasing temperatures,  $\text{B}_2\text{O}_3$  forms a solid solution ( $9\text{Al}_2\text{O}_3\text{-}2\text{B}_2\text{O}_3$ ) with the  $\text{Al}_2\text{O}_3$  surface layer on the Al particles. The Al continues to expand and eventually breaks or pushes out of the  $\text{Al}_2\text{O}_3$  surface layer, exposing fresh Al. This happens because the coefficient of thermal expansion of Al is much greater than that of the  $\text{Al}_2\text{O}_3$ . At the temperature corresponding to the melting point of Al ( $T_m = 660^\circ \text{C}$ ), the fresh metal melts and oxidizes.  $\text{Al}_2\text{O}_3$  is formed continuously while B and Ti are reduced by the aluminum from their oxide precursors. Once the Ti and B are free, the  $\text{TiB}_2$  phase forms. A similar, though somewhat simpler, double reduction process has been associated with the three-component system of Al, C, and  $\text{TiO}_2$  (Chrysathou et al. 1994; Kim and Lee 1989).

With a brief description of the reaction process in mind, results of the temperature-time measurements in the reaction fixture can now be discussed. Figure 4 shows the thermocouple and pyrometer data. The thermocouple reaction velocity data are shown in Figure 4A, and the pyrometer temperature data are illustrated in Figure 4B. In Figure 4A, the open and closed squares represent the thermocouples at the sample's top while the open and closed circles represent the thermocouples at the sample's bottom. As revealed by the very short time interval between the appearance of the open and closed squares, the reaction wavefront propagates

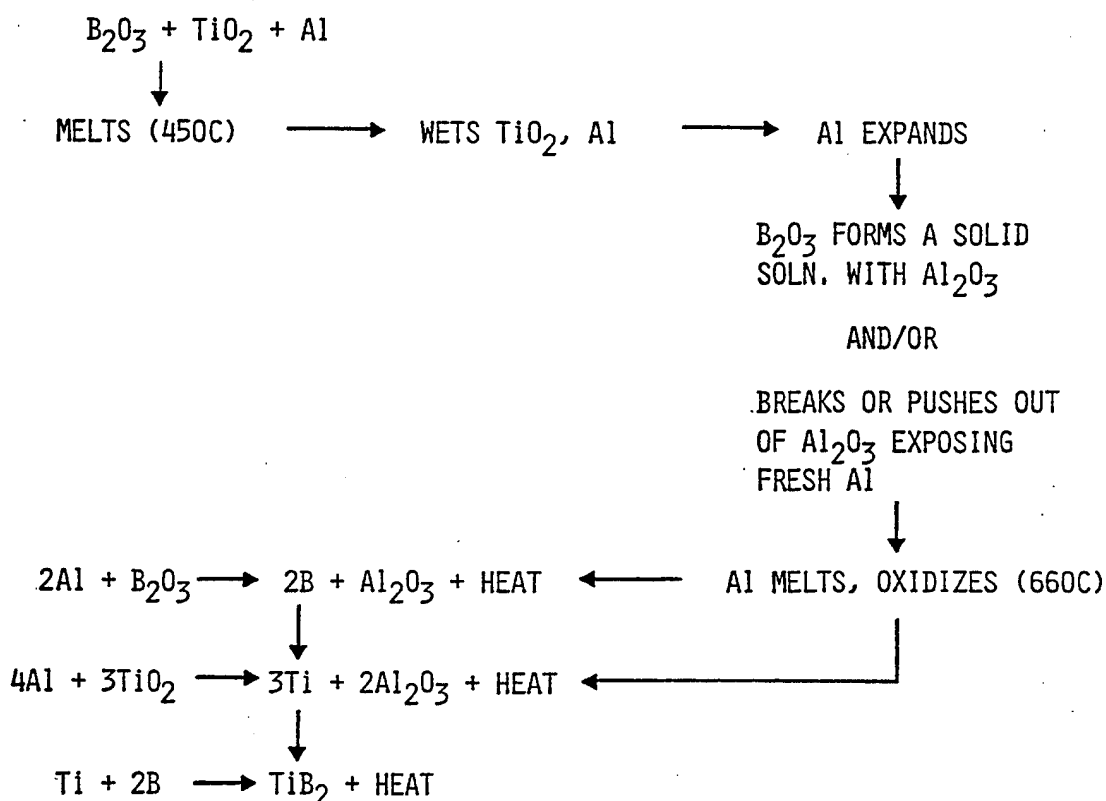
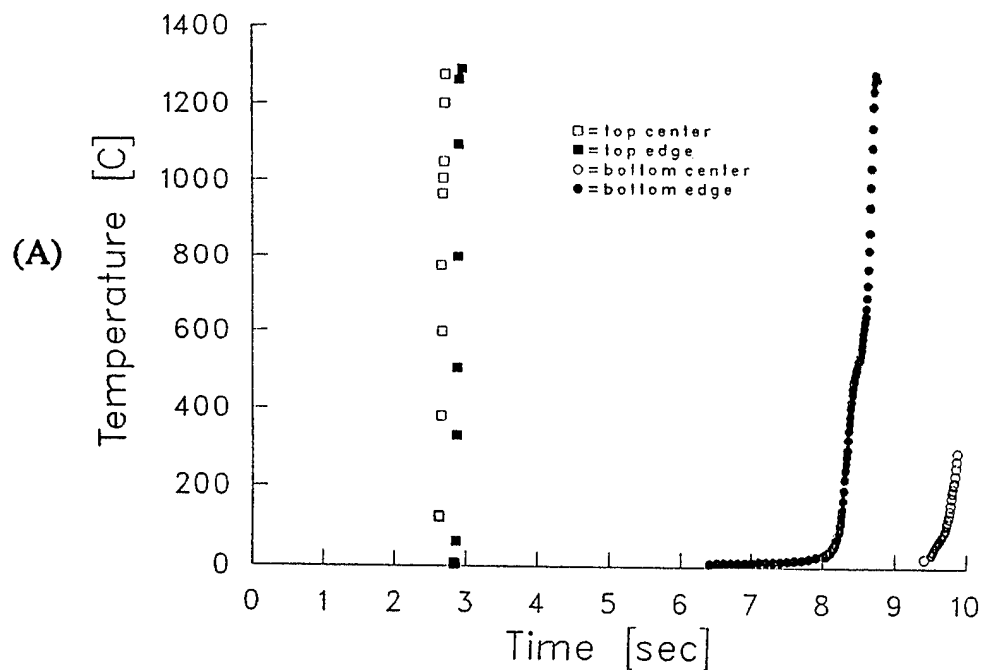


Figure 3. Diagrammatic representation of the  $\text{Al}_2\text{O}_3$ - $\text{TiB}_2$  reaction process.

quickly (0.2 s) from the center of the igniter mixture to the edge of the compact. It was presumed that once the entire top surface of the compact is ignited, the CS reaction, approximating a planar wave, propagates downward, consuming the unreacted material. However, as is apparent from this figure, when the reaction front reaches the bottom of the green compact, the edge thermocouple exceeds its rated temperature range approximately 1.5 s ahead of the center one. This implies that the reaction front arrived at the bottom edge 1.5 s earlier than at the bottom center. The reaction velocity ranges approximately from 0.34 cm/s at the core to 0.40 cm/s at the edge, which corresponds to a relatively slow reaction. In Figure 4B, the pyrometer data reflect a maximum surface temperature of 1,750° C, which is below the melting points of both  $\text{Al}_2\text{O}_3$  ( $T_m = 2,050^\circ \text{C}$ ) and  $\text{TiB}_2$  ( $T_m = 3,190^\circ \text{C}$ ). In this figure, the top center thermocouple data (open squares) is included for reference. Furthermore, the data shows that the

Contained Run of Al<sub>2</sub>O<sub>3</sub>-TiB<sub>2</sub> Composite



Contained Run of Al<sub>2</sub>O<sub>3</sub>-TiB<sub>2</sub> Composite

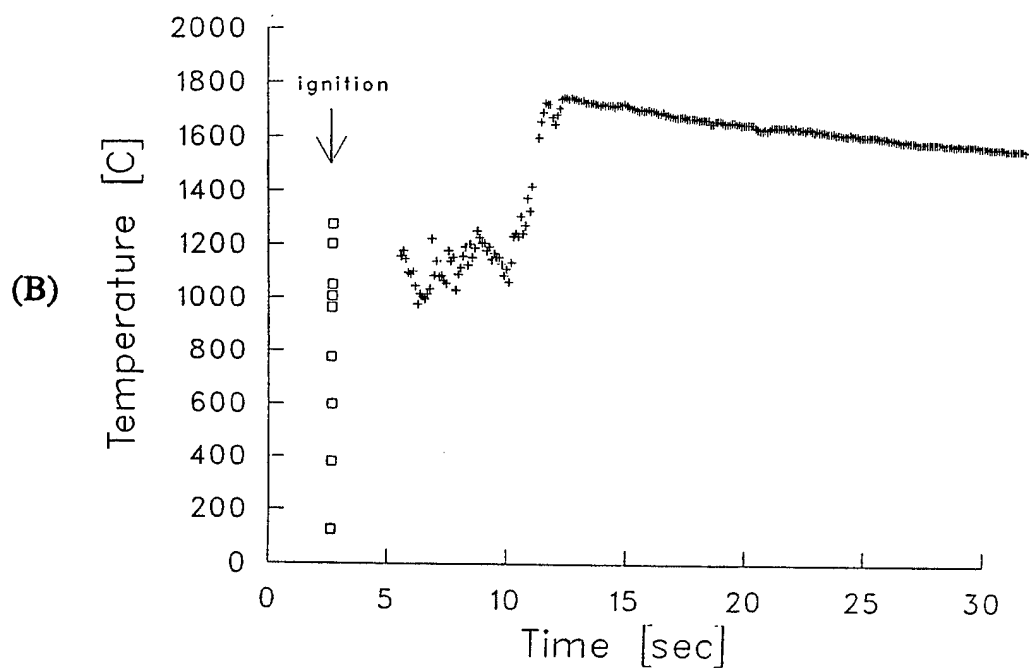


Figure 4. Temperature data for the Al<sub>2</sub>O<sub>3</sub>-TiB<sub>2</sub> system. Thermocouple data are shown in 4A, and pyrometer data are shown in 4B.

product cools very slowly. In fact, the surface remains above 1,200° C for at least 80 s, and at this temperature, the sample is still above the 1,000° C ductile-brittle transition temperature (DBTT) of  $\text{Al}_2\text{O}_3$ , although it is below the DBTT of  $\text{TiB}_2$ , 1,800° C.

The complexity of the three-component reaction process is reflected in the thermocouple and pyrometer traces. In particular, the thermocouples show that a primary reaction wave propagates through the compact in approximately 7.5 s. At 3 s after ignition, the pyrometer turns on in agreement with the speed of the primary wave. After a widely oscillatory behavior for 5 s, the peak temperature is reached at about 10 s after ignition. This is 2 s after the primary wave already passed through the entire compact. Recall that the pyrometers are pointed at the midline of the compact. This 2-s delay implies that the reaction takes several additional seconds to complete. Therefore, it may be concluded that the entire compact has reacted about 15 s after ignition.

It is very tempting to associate the pyrometer data with the various intermediate steps in the reaction process. Caution must be exercised, however. Specifically, during the intermediate stages of the reaction, the compact emits light, and the characteristic emission lines could well be in the optical frequency band of the pyrometer where the blackbody temperature is determined. Without an independent measurement of the emission spectrum of this system, and until true blackbody behavior is established, the association of an actual physical process with the pyrometer temperature traces should be avoided.

After the in-situ temperature measurement, the reacted (but uncompact) product or sponge was sectioned for analysis. The polished cross section of the reacted sponge and enlarged views of characteristic regions are shown in Figure 5. The macrophotograph in Figure 5A clearly shows that, at the top of the sponge, the periodic delaminations are parallel to one another. At the bottom, however, the delaminations have a pronounced curvature. This is consistent with the previously discussed thermocouple data, where the thermocouple at the sample's bottom edge registered the wave front arrival about 1.5 s before the thermocouple at the sample's bottom center. The increased speed along the surface of the compact is probably caused by a difference

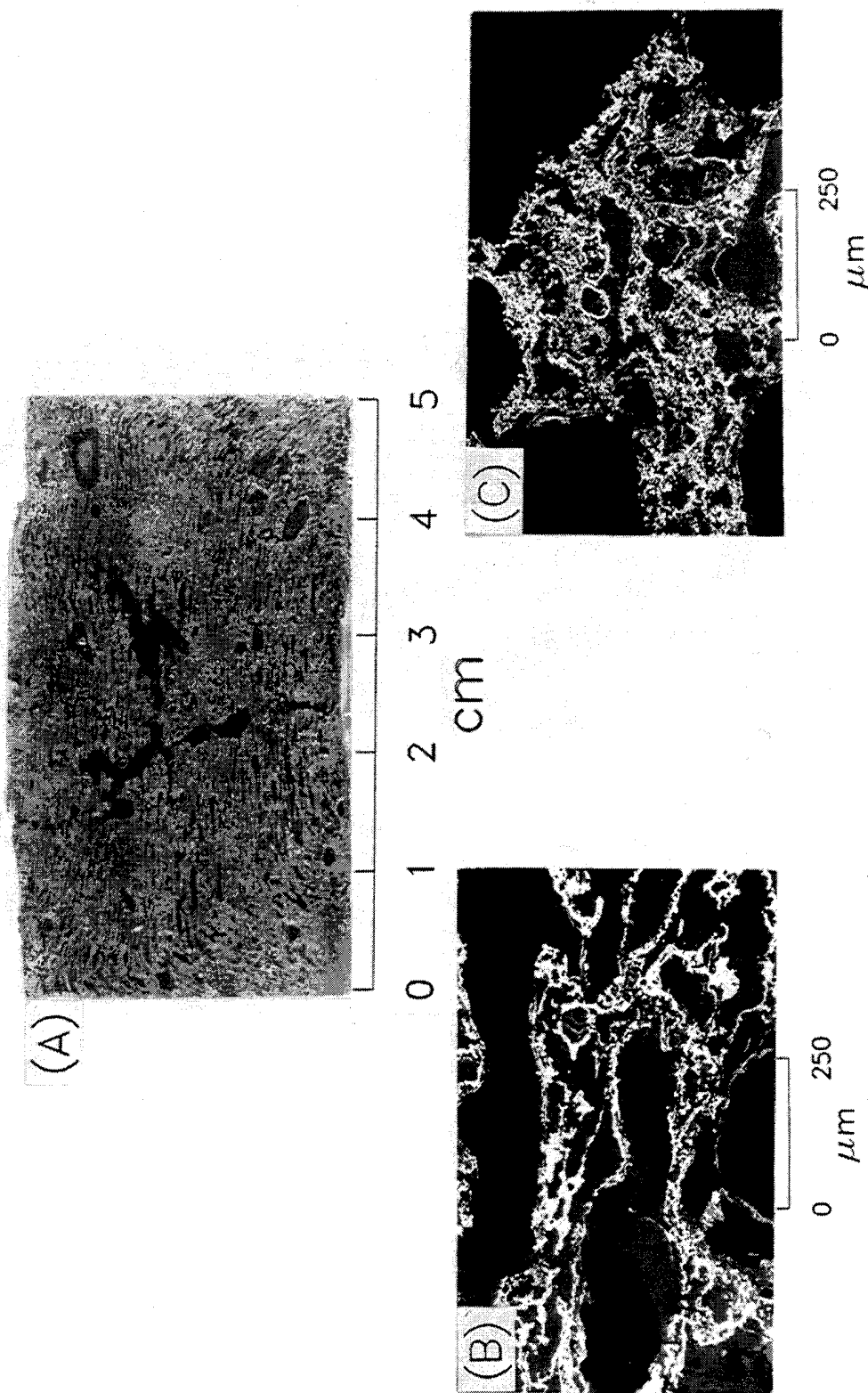


Figure 5. Macro photograph of the reacted, but uncompacted sample in 5A, with enlargements of typical microstructural features in 5B and 5C.

in the amount of oxygen available for the formation of  $\text{Al}_2\text{O}_3$ . Whereas at the center, oxygen can come only from the  $\text{B}_2\text{O}_3$  and  $\text{TiO}_2$ , while at the edge, oxygen to form  $\text{Al}_2\text{O}_3$  can come from  $\text{B}_2\text{O}_3$ ,  $\text{TiO}_2$ , and the air in the reaction fixture.

The large voids interrupting the periodic delaminations of the sponge are a cause for concern. These voids appear throughout the reacted sponge, with a higher concentration at the center. The macrovoids are probably caused by the rapid melting and vaporization of the  $\text{B}_2\text{O}_3$  (Logan, Price, and McLemore 1987; Logan, Sparrow, and McLemore 1990). Figures 5B and 5C are backscattered electron micrographs of typical regions found in the sample. The white regions are  $\text{TiB}_2$ , the lighter grey regions are  $\text{Al}_2\text{O}_3$ , and the dark grey-to-black regions are voids. The  $\text{TiB}_2$  phase consists of individual hexagonal, platelet-like crystals dispersed in the  $\text{Al}_2\text{O}_3$  phase. The dispersion consists of isolated crystals, crystal aggregates, and continuous, swirling bands of very fine crystallites. These crystallite bands are most likely a direct result of the very fine  $\text{TiO}_2$  particles adhering to the surface of the Al particles.

**3.2 CS/DC Experiments.** The CS/DC experiments in the  $\text{Al}_2\text{O}_3$ - $\text{TiB}_2$  composite system were conducted in a manner much like the empirical approach used in the CS/DC of the TiC and  $\text{TiB}_2$  systems (Niiler et al. 1988; Niiler, Kecskes, and Kottke 1990). Preliminary experiments in which delay times were less than 5 s revealed that during consolidation, especially at higher c:m values (i.e., 0.33 and 0.44), the  $\text{Al}_2\text{O}_3$ - $\text{TiB}_2$  ceramic spread beyond the confines of the steel retaining ring, resulting in an inferior product. It was concluded that the poor results from the use of this reaction/consolidation configuration were caused by three factors: (1) the unusually long duration of the SHS reaction, (2) the relatively low melting point of the  $\text{Al}_2\text{O}_3$  phase, and (3) slower cooling caused by the low thermal conductivity of  $\text{Al}_2\text{O}_3$ . Consequently, it was postulated that densification could be improved if the product's stiffness was increased. In the thermally passive reaction/consolidation fixture, this could be simply accomplished by allowing the sample to cool through a longer delay time than used in previous experiments.

The CS/DC samples were about 12 mm thick and 51 mm in diameter. A typical sample is shown in Figure 6 with the steel retaining ring, Grafoil barrier, and some zirconia insulation still

Top view



(A)

Bottom view



(B)

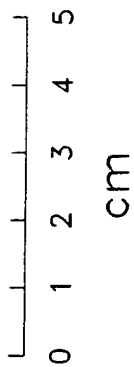


Figure 6. Typical CS/DC  $\text{Al}_2\text{O}_3$ - $\text{TiB}_2$  sample with top and bottom views shown in 6A and 6B, respectively.

adhering to the ceramic. Figures 6A and 6B show the top and bottom views, respectively. The CS/DC sample densities and microhardnesses are tabulated in Table 1. Also included in the table are the delay time, or  $t_d$ , and the sample temperature,  $T_c$  (as inferred from the auxiliary measurement), at the time of consolidation.

Table 1.  $\text{Al}_2\text{O}_3$ - $\text{TiB}_2$  Sample Density and Microhardness

Sample	$t_d^a$ (s)	$T_c^b$ (°C)	Density (g/cm <sup>3</sup> )	HK	
				100-g (GPa)	400-g (GPa)
S59	4.2	1,100	2.37	25.5 ±1.3	17.1 ±1.2
S54	11.4	1,700	2.74	29.4 ±2.2	14.9 ±0.8
S57	12.1	1,700	2.64	29.4 ±2.6	14.6 ±0.6
S58	16.8	1,650	3.03	26.2 ±2.3	13.7 ±0.7
S60	38.9	1,480	3.60	23.6 ±1.6	13.6 ±0.6
S61	58.8	1,390	3.55	26.3 ±2.0	14.3 ±0.6

<sup>a</sup> Reaction ignition-consolidation delay time.

<sup>b</sup> Sample temperature at time of consolidation (from auxiliary measurement).

Because the product sponge remains at elevated temperatures for an extended period of time, the possibility of thermal decomposition of the  $\text{Al}_2\text{O}_3$  and  $\text{TiB}_2$  phases must be addressed. XRD analysis identified the major phases as  $\alpha$ - $\text{Al}_2\text{O}_3$  and  $\text{TiB}_2$  and detected the presence of small amounts of  $\alpha$ - $\text{SiO}_2$ . The results are summarized in Table 2. No peaks from the precursors were observed. The samples may still have been subject to thermal decomposition, but, if so, the effect was below the XRD detection limit. The tabulated values represent the ratio of the principal peak intensity of each of the listed phases to that of  $\text{TiB}_2$ . The average intensity ratio of the two major phases (most intense peak) is  $0.68 \pm 0.10$ . The larger deviation of the ratio for the S60 sample is not understood. The peak intensity of  $\text{SiO}_2$ , however, generally decreases with increasing delay time and sample density. The source of  $\text{SiO}_2$  is discussed later.

Table 2. X-ray Diffraction Results of  $\text{Al}_2\text{O}_3\text{-TiB}_2$  Samples

Sample	$T_d$ (s)	Peak Intensity Ratio		
		$\text{TiB}_2$	$\text{Al}_2\text{O}_3$	$\text{SiO}_2$
S59	4.2	1.00	0.77	0.10
S54	11.4	1.00	0.63	0.20
S57	12.1	1.00	0.72	0.12
S58	16.8	1.00	0.70	0.10
S60	38.9	1.00	0.48	0.07
S61	58.8	1.00	0.78	0.04

Based on the XRD data, it is not unreasonable to assume that sample composition remains thermally stable with time. If the composites' compositions do not change, then their densities can be normalized to a single theoretical density. The results shown in Figure 7 indicate an improvement from less than 60% to close to 90% of the theoretical density. It may be noted that a similar but lesser effect was found in the consolidation of  $\text{TiC}$  (Grebe et al. 1992). The horizontal line in the figure represents  $4.14 \text{ g/cm}^3$ , the theoretical density of the composite. Most of the increase in density occurs between delay times of 4 and 30 s, leveling off at longer  $t_d$ .

Macrophotographs of the polished cross sections from the CS/DC samples are shown in Figure 8. From the figure, the consolidated product structures can be grouped into three categories. In the first, for delay times less than the time at which the peak temperature is reached,  $t_p$  (as apparent in the sample consolidated at 4.2 s), the sample still retains a generally laminar profile. (Note: In Figure 4, the peak temperature of  $1,750^\circ \text{C}$  is attained at a delay time of 10 s.) In the second, for a  $t_d$  between  $t_p$  and 20 s, the smaller lenticular voids of the product sponge coalesce into larger macro-voids, while at the same time, an outer, denser zone begins to form (see samples consolidated at 11.4, 12.1, and 16.8 s). For  $t_d$  values longer than 20 s, the relative amount of this zone continues to increase, but the interior of the sample, even at 38.9 s, remains quite porous. Finally, at 58.8 s, the sample contains no macro-voids and appears to be

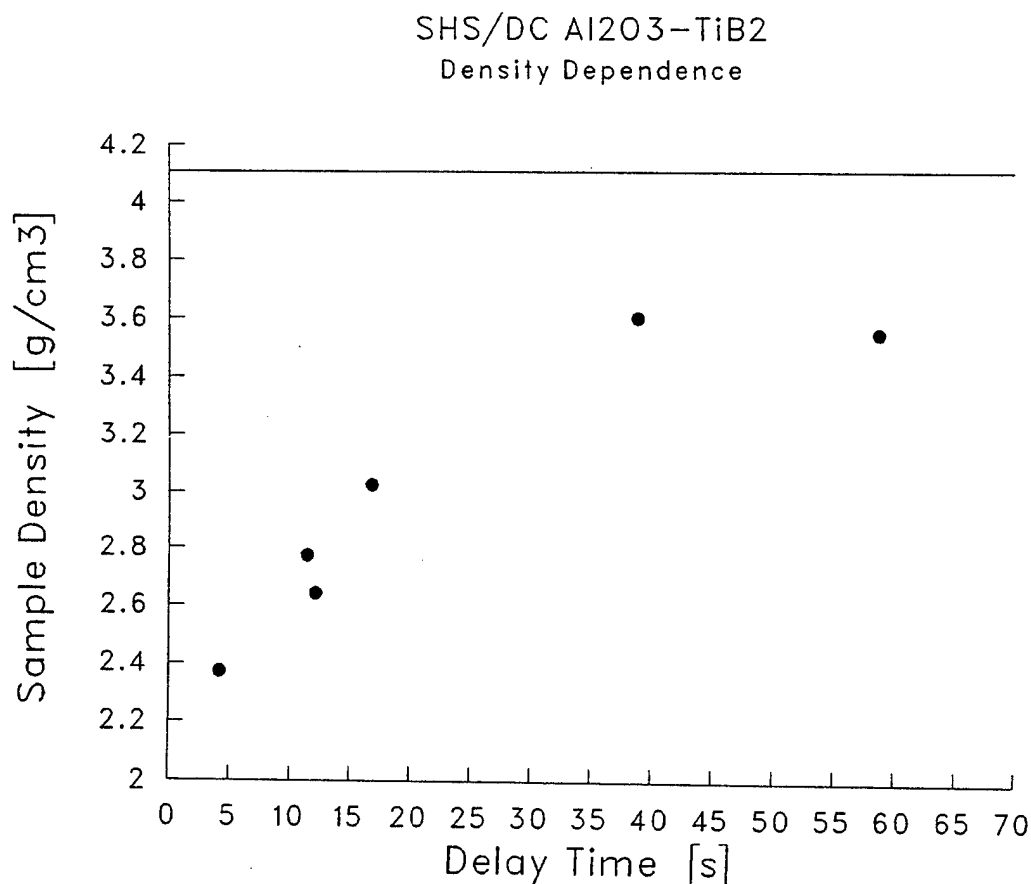


Figure 7.  $\text{Al}_2\text{O}_3\text{-TiB}_2$  sample density vs. delay time.

solid. It is interesting to note that the sample densities at 38.9 s and 58.8 s are about the same. A possible explanation of this fact may be that the 38.9-s sample contains higher levels of open porosity.

As shown in Figure 9, backscattered electron micrographs of central regions of the samples are in fairly good agreement with the observation of the overall product development. An explanation of the laminar structure of the sample consolidated at 4.2 s (see Figure 9A) is quite straightforward. At the time of consolidation, the combustion synthesis reaction is still ongoing

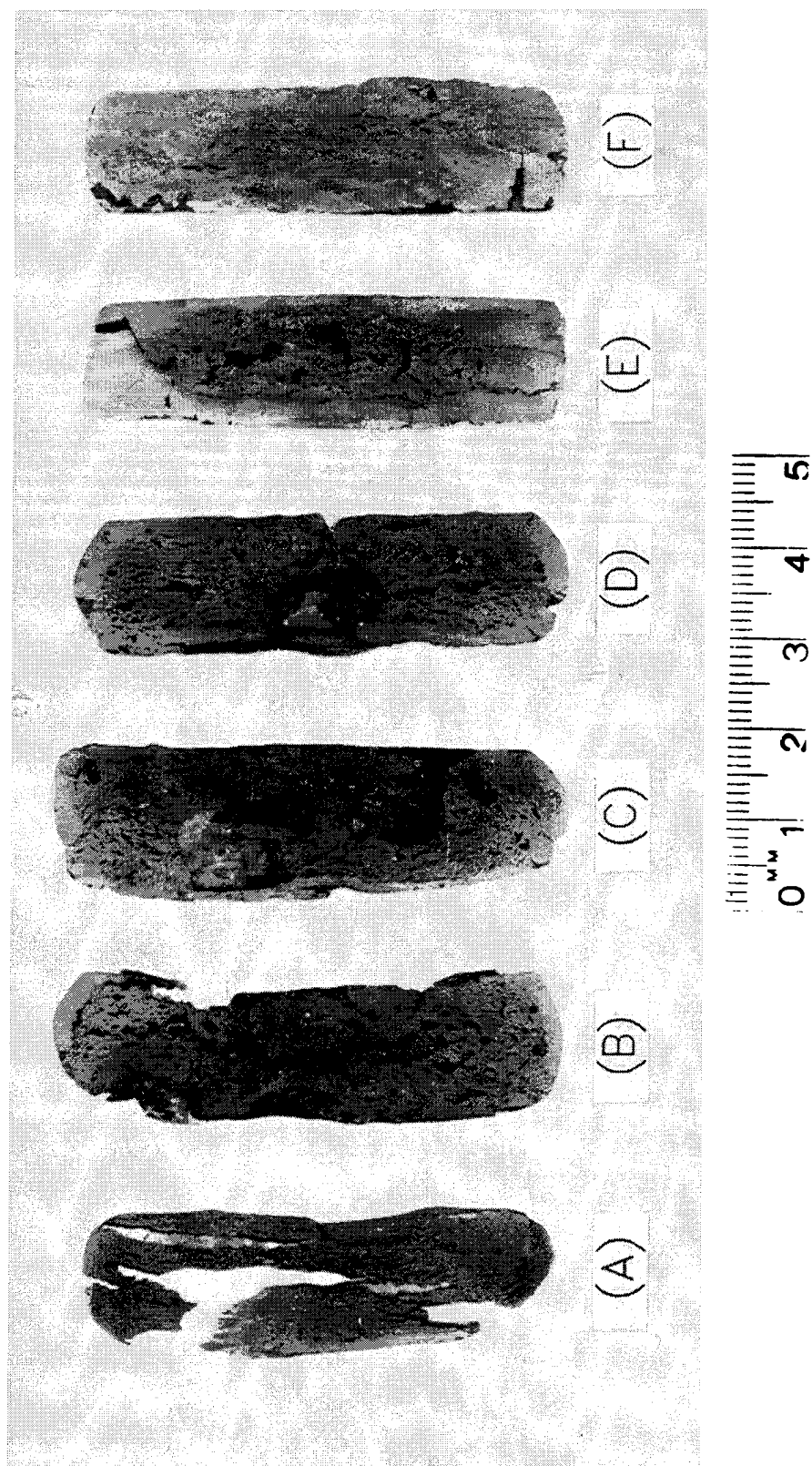


Figure 8. Optical macrophotographs of polished cross sections of the samples with a  $t_d$  of 4.2 s in 8A, 11.4 s in 8B, 12.1 s in 8C, 16.8 s in 8D, 38.9 s in 8E, and 58.8 s in 8F.

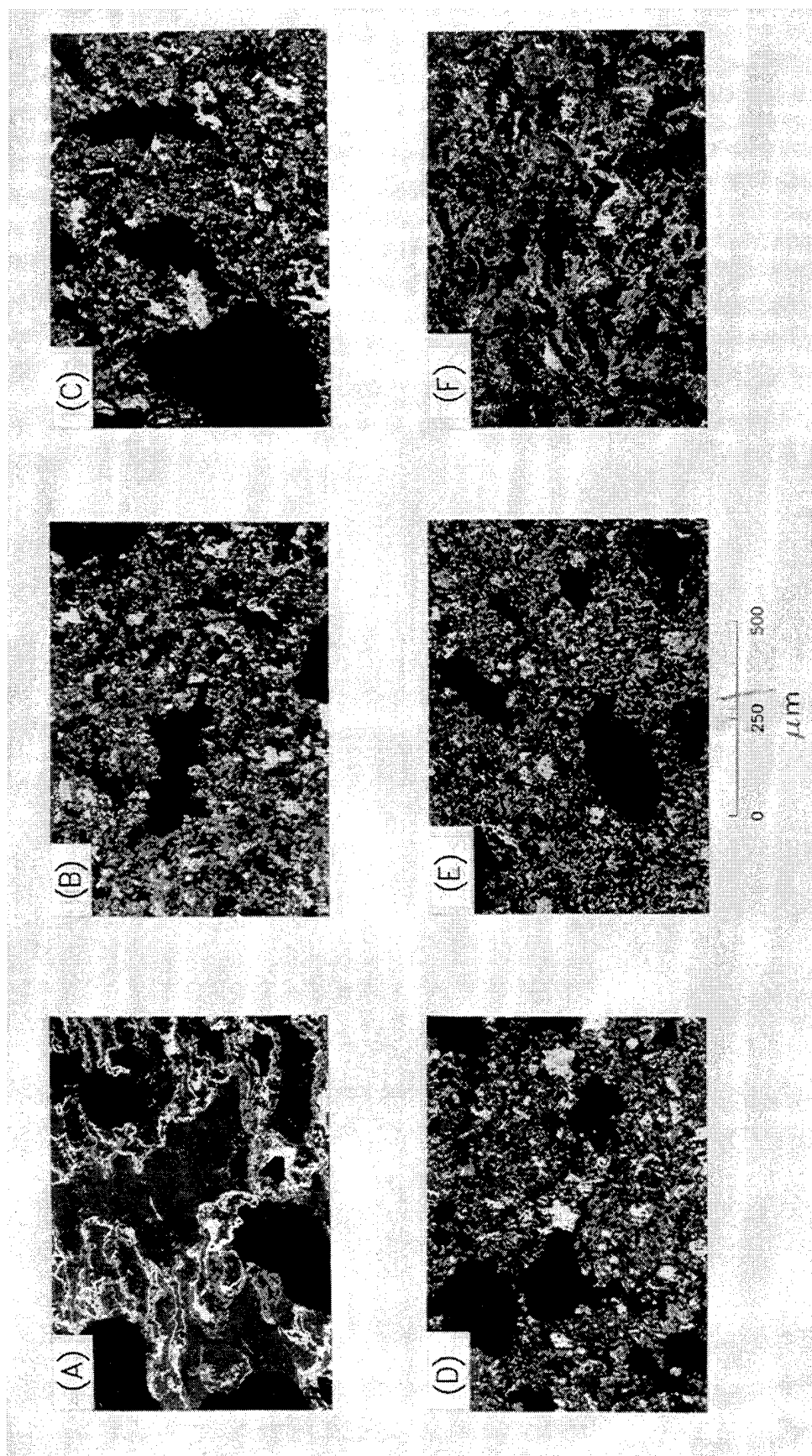


Figure 9. Backscattered electron micrographs of the  $\text{Al}_2\text{O}_3\text{-TiB}_2$  samples with a  $t_d$  of 4.2 s in 9A, 11.4 s in 9B, 12.1 s in 9C, 16.8 s in 9D, 38.9 s in 9E, and 58.8 s in 9F.

and continues after the consolidation event, leaving the characteristic laminar structure of the uncompacted product sponge. In the four intermediate samples, Figures 9B, 9C, 9D, and 9E, the  $\text{TiB}_2$  crystals are dispersed differently. The fine bands of  $\text{TiB}_2$  swirls are absent, and the crystals are now found in aggregates only. With the temperature rise generated during consolidation, the  $\text{Al}_2\text{O}_3$  phase may undergo melting that causes the fine bands of  $\text{TiB}_2$  crystals to coalesce into larger aggregates. As shown in Figure 9F, at the other extreme of the time scale (at 58.8 s), the swirling pattern is again more dominant. Possibly, at a  $t_d$  of 58.8 s, the sample has cooled further and the additional shock energy is able to close the open porosity of the uncompacted sponge but is insufficient to bring about a change in the distribution of either phase.

The segregation and distribution of the  $\text{TiB}_2$  phase in the CS/DC samples not only depends on the delay time but also varies with location in the sample. A comparison of the edge to the central region of one of the intermediate density samples (S60) is shown in Figure 10. In the uncompacted product sponge, the  $\text{TiB}_2$  bands and small aggregates appeared everywhere. From this figure, it is clear that during consolidation a separation occurs. At the center of the sample (Figure 10A), there are  $\text{TiB}_2$  aggregates only, but at the edge (Figure 10B), the band pattern of finer  $\text{TiB}_2$  grains is more dominant. The spatial separation may be explained in terms of the local heat content of the samples. In the cooler edge zones, due to greater heat losses to the surroundings, neither phase can melt to allow recrystallization. In contrast, at the center, heat is retained longer and segregation could occur. That is, while the  $\text{Al}_2\text{O}_3$  phase at the edges is only ductile, at the center it may be flowing plastically. The smaller degree of aggregation is probably the reason for the decreased porosity at the edges relative to the center of the sample. The smaller  $\text{TiB}_2$  grains are easier to displace during consolidation than the larger aggregates. This, in turn, may account for the more uniform profile of the sample consolidated at 58.8 s.

The mechanical integrity of the CS/DC  $\text{Al}_2\text{O}_3$ - $\text{TiB}_2$  samples was assessed by SEM examination of fracture surfaces and by microhardness measurements. As shown in Figure 11, the failure mode of the samples does not change significantly with increasing delay times. This is evident in the transgranular fracture of the  $\text{Al}_2\text{O}_3$  grains (dark grey) and the intergranular fracture between  $\text{TiB}_2$  grains (white to light grey). (Note that in all three samples the  $\text{Al}_2\text{O}_3$

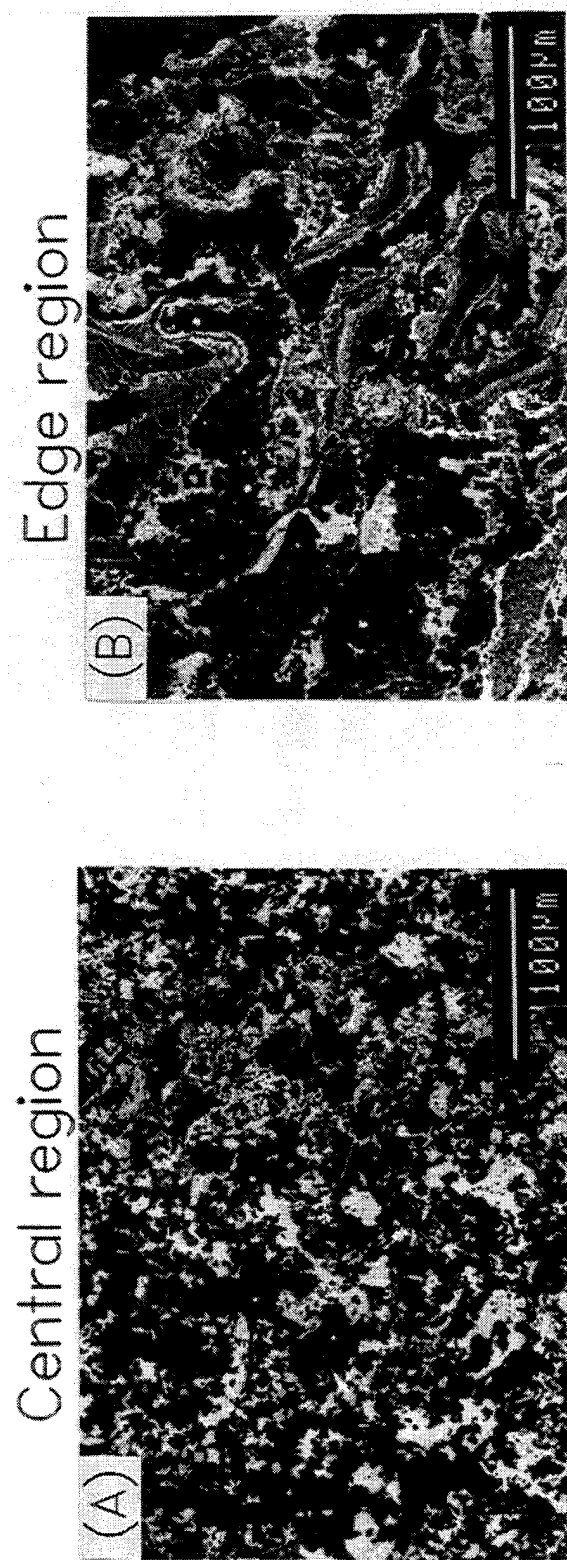


Figure 10. Degree of aggregation and intermixing of the  $\text{Al}_2\text{O}_3$  and  $\text{TiB}_2$  phases in the S60 (38.9 s) sample. The central region is shown in 10A, and the edge is shown in 10B.

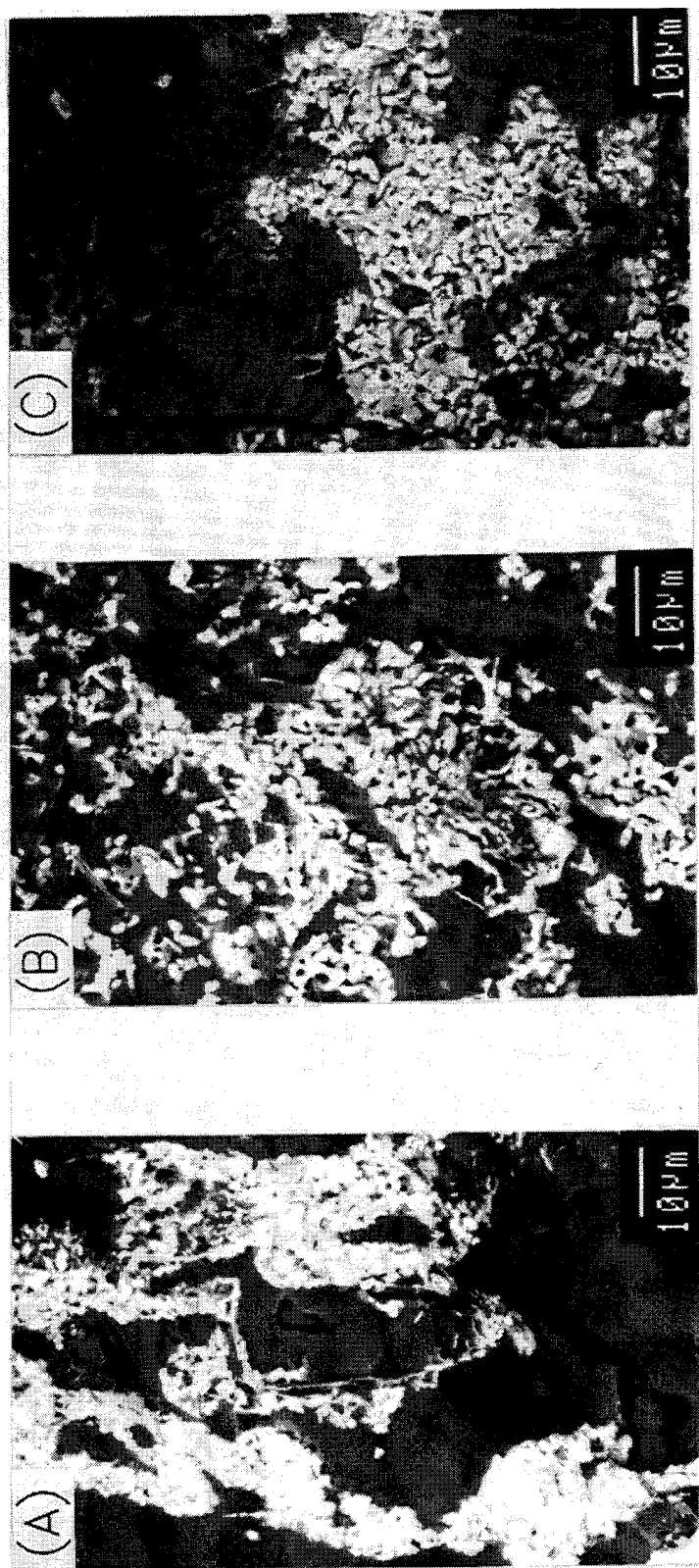


Figure 11. Characteristics fracture surfaces of the  $\text{Al}_2\text{O}_3\text{-TiB}_2$  samples. The S59 (4.2 s) sample shown in 11A, the S57 (1.4 s) sample in 11B, and the S60 (38.9 s) sample in 11C.

grains failed in the transgranular mode, nevertheless, the appearance of the grain surfaces can range from those of being cleaved to those of being striated.) The intergrain bonding of the  $\text{Al}_2\text{O}_3$  phase appears to be stronger than that of the  $\text{TiB}_2$  phase. The intergranular separation of the  $\text{TiB}_2$  grains reveals small pores trapped between the individual  $\text{TiB}_2$  crystals of the aggregate. Also note the small amount of sintering and lack of grain growth within the  $\text{TiB}_2$  aggregates.

These aggregates contain individual  $\text{TiB}_2$  crystals that are an order of magnitude smaller than the  $\text{Al}_2\text{O}_3$  grains. This large size difference between the  $\text{TiB}_2$  and  $\text{Al}_2\text{O}_3$  is mainly caused by the size of the  $\text{TiO}_2$  precursor. Because of its low melting point, Al is liquid at the reaction temperatures. Therefore, it is expected that its size will not affect the size of the  $\text{Al}_2\text{O}_3$  grains (Logan, Price, and McLemore 1987; Logan, Sparrow, and McLemore 1990). However, as evident in Figures 1 and 11, the size of the  $\text{TiO}_2$  particles has a strong influence on the size of the  $\text{TiB}_2$  grains. Due to the constraints imposed by the rapid post-consolidation cooling, the relatively low temperatures attained in the CS/DC fixture, and the high melting point of  $\text{TiB}_2$ , grain growth is likely to be limited. While a fine-grained composite is highly desirable, small grains may not develop strong intergranular bonding if there are impurities present or insufficient heat is available for sample sintering.

As expected, Knoop microhardness measurements yielded values that are considerably higher than those of pure  $\text{Al}_2\text{O}_3$  but much lower than those of pure  $\text{TiB}_2$ . With increasing delay time, there is a slight decrease in both 100-g and 400-g hardness values. The reduction in microhardness may be due to a possible weakness of intergranular bonds between the  $\text{TiB}_2$  crystals. It is speculated that the weaker bonding of the samples with longer delay times may be caused by two concurrent factors. First, at elevated temperatures, the porous sponge is highly susceptible to contamination from external sources. Small amounts of impurities are known to degrade the mechanical properties of hard solids (Kny and Ortner 1986). Likewise, after consolidation, if still porous, the CS/DC sample continues to remain vulnerable to contamination. Second, although generally inhibited by the presence of  $\text{Al}_2\text{O}_3$ , the high-temperature oxidation of  $\text{TiB}_2$  in air is thermodynamically favored (Matasushita, Hayashi, and Saito 1990; Tampieri, Landi, and Bellosi 1992; Cutler, Hurford, and Virkar 1989; Ishigaki, Sato, and Moriyoshi 1989).

That is, intergrain bond degradation can be caused by the incomplete conversion of reactants to products.

Evidence of these factors is found by XRD analysis as well as SEM/EDS examination of the samples. Typical examples of contamination and nonuniformity are shown in Figure 12. A backscattered electron micrograph of a  $\text{TiB}_2$  aggregate is shown in Figure 12A. The bright grain boundary regions are trapped foreign species. EDS spot analysis identified Zr, Si, and Fe. The source of Si, of course, is the sand from the sandpile used in the compaction experiments. Recall that the normalized peak intensity of  $\alpha\text{-SiO}_2$  decreases with increasing density or, conversely, with decreasing porosity (see Table 2). As expected, a decrease in the residual porosity decreases the contamination. Fe is also likely to be from the sand, while Zr is probably from the  $\text{ZrO}_2$  felt. A backscattered electron micrograph in Figure 12B illustrates another type of nonuniformity found within some of the  $\text{TiB}_2$  grain clusters. While this figure appears much like that shown in Figure 12A, EDS spot analysis of the bright grain boundary regions detected Ti only. Neither B nor O can be detected in the EDS analyzer because their characteristic x-rays are absorbed in the detector window. However, because brighter regions correspond to higher average atomic number in a backscatter image, it may be concluded that these regions are most likely  $\text{TiO}_2$ . Possible sources of excess  $\text{TiO}_2$  could be either trapped, unreacted precursor powder remnants or the result of surface oxidation of the microfine  $\text{TiB}_2$  grains.

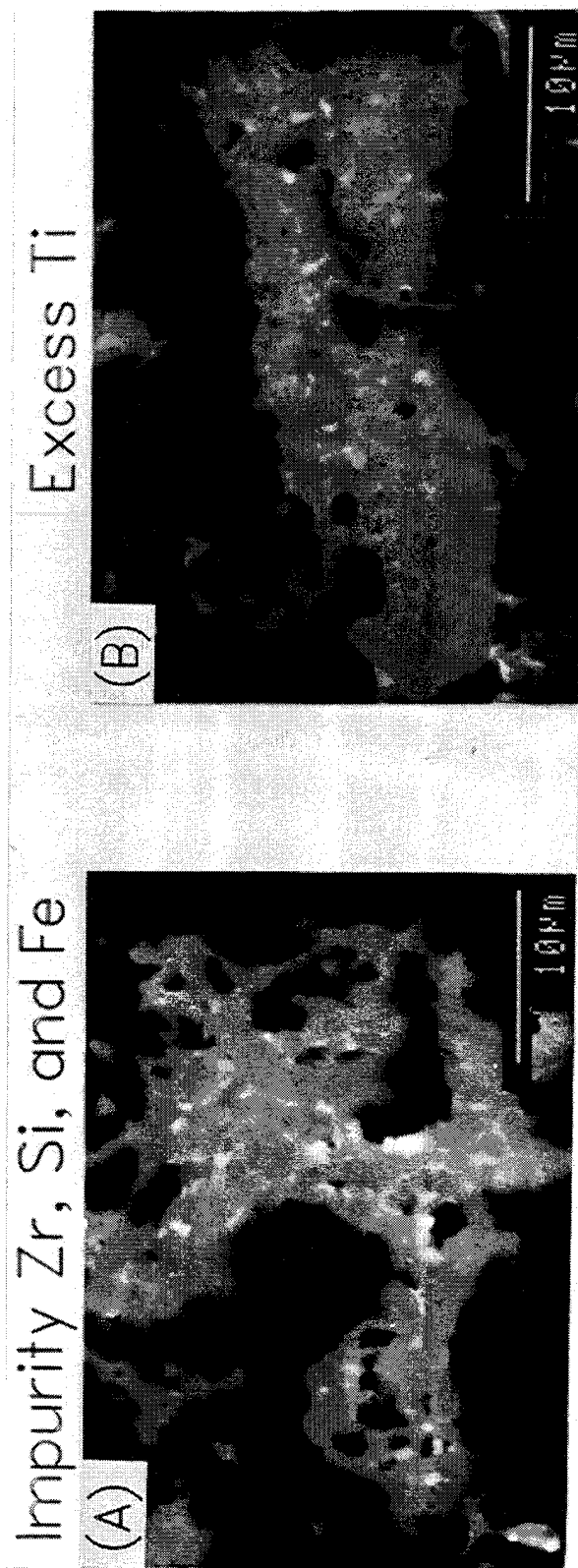


Figure 12. Inhomogeneity of the  $\text{Al}_2\text{O}_3\text{-TiB}_2$  samples. External contamination is shown in 12A, and incomplete conversion of reactants to products is shown in 12B.

#### 4. CONCLUSIONS

It has been demonstrated that the CS/DC technique, developed for TiC and TiB<sub>2</sub> systems, can also be applied to the Al<sub>2</sub>O<sub>3</sub>-TiB<sub>2</sub> ceramic system. Due to the large difference between the melting points of the Al<sub>2</sub>O<sub>3</sub> and TiB<sub>2</sub> phases, the latter system presents more difficulties and does not correlate well with the former systems. That is, the applicability of the critical process variables, identified for TiC and TiB<sub>2</sub>, is significantly restricted. Sample densities of 90% TD can be attained by varying the reaction ignition-consolidation delay time. The measurement of the temperature-time history of the combustion synthesis reaction and an understanding of the reaction mechanism are necessary to determine the appropriate delay time for maximizing the sample density. Successful consolidation of the Al<sub>2</sub>O<sub>3</sub>-TiB<sub>2</sub> composite ceramic depends on the capacity of the ceramic to cool sufficiently so that it shifts from the plastic into the ductile deformation regime.

These CS/DC samples consist of a continuous Al<sub>2</sub>O<sub>3</sub> phase and a much finer, well-dispersed phase of TiB<sub>2</sub> single crystal clusters. The TiB<sub>2</sub> grain size is found to be strongly linked to that of the precursor TiO<sub>2</sub>. Samples exhibit relatively high hardness values, but, as reflected in the incongruent failure mode of the Al<sub>2</sub>O<sub>3</sub> and TiB<sub>2</sub> phases, intergrain bonding is relatively weak. The less-than-adequate intergrain bonding is related to the residual porosity and resultant high sensitivity of the CS/DC sample to post-compaction contamination from surrounding insulating media and sand. The intergrain bonding and limited grain growth of the TiB<sub>2</sub> crystals demonstrate that the overall effect of contaminant phases is to weaken intergrain bonding by the prevention of sintering and grain growth.

Several modifications can easily be proposed to improve sample characteristics. An increase in sample density could be accomplished by using of higher c:m values coupled with the strengthening of the confinement fixture. Similarly, further dispersion of the TiB<sub>2</sub> phase and the control of the TiB<sub>2</sub> grain size could be achieved by improved precursor mixing and using larger TiO<sub>2</sub> precursor powder. An improvement in the fixture design to significantly reduce contamination from external sources would greatly improve the utility of the CS/DC process to fabricate Al<sub>2</sub>O<sub>3</sub>-TiB<sub>2</sub> ceramics.

## 5. REFERENCES

- Adachi, S., T. Wada, T. Mihara, Y. Miyamoto, and M. Koizumi. "High-Pressure Self-Combustion Sintering of Alumina-Titanium Carbide Ceramic Composite." J. Am. Ceram. Soc., vol. 73, no. 5, pp. 1451-1452, May 1990.
- Adachi, S., T. Wada, T. Mihara, M. Koizumi, and O. Yamada. "Fabrication of Titanium Carbide Ceramics by High-Pressure Self-Combustion Sintering of Titanium Powder and Carbon Fiber." J. Am. Ceram. Soc., vol. 72, no. 5, pp. 805-809, May 1989.
- Chrysathou, A., A. Saidi, C. E. W. Aylott, and J. V. Wood. "Preparation and Microstructure of  $\text{Al}_2\text{O}_3$ -TiC Composites by Self-Propagated High Temperature Synthesis." J. Alloys and Compounds, vol. 203, nos. 1-2, pp. 127-132, January 1994.
- Cutler, R. A., A. C. Hurford, and A. V. Virkar. "Pressureless-Sintered  $\text{Al}_2\text{O}_3$ -TiC Composites." Int. J. Refract. Hard. Met., vol. 8, no. 2, pp. 114-120, June 1989.
- Furukawa, M., O. Nakano, and Y. Takashuna. "Fracture Toughness of  $\text{Al}_2\text{O}_3$ -TiC Ceramics." Int. J. Refract. Hard. Met., vol. 7, no. 1, pp. 37-40, March 1988.
- Grebe, H. A., A. Advani, N. N. Thadhani, and T. Kottke. "Combustion Synthesis and Subsequent Explosive Densification of Titanium Carbide." Met. Trans. A, vol. 23A, no. 9, pt. 2, pp. 2365-2372, September 1992.
- Hoke, D. A., M. A. Meyers, L. W. Meyer, and G. T. Gray. "Reaction Synthesis/Dynamic Compaction of Titanium Diboride." Met. Trans. A, vol. 23A, no. 1, pt. 1, pp. 77-86, January 1992.
- Ishigaki, T., K. Sato, and Y. Moriyoshi. "Pressureless Sintering of TiC- $\text{Al}_2\text{O}_3$  Composites." J. Mat. Sci. Lett., vol. 8, no. 6, pp. 678-680, June 1989.
- Kecskes, L. J., T. Kottke, P. H. Netherwood, Jr., R. F. Benck, and A. Nüiler. "Explosive Consolidation of Combustion Synthesized  $\text{TiB}_2$  and TiC; Microstructural Properties." BRL-TR-3133, U.S. Army Ballistic Research Laboratory, Aberdeen Proving Ground, MD, 1990.
- Kecskes, L. J., A. Nüiler, and T. Kottke. "Microstructural Properties of Combustion-Synthesized and Dynamically Consolidated Titanium Boride and Titanium Carbide." J. Am. Ceram. Soc., vol. 73, no. 5, pp. 1274-1282, May 1990.
- Kecskes, L. J., A. Nüiler, and T. Kottke. "Precursor Morphology Effects in Combustion-Synthesized and Dynamically Consolidated Titanium Carbide and Titanium Boride." J. Am. Ceram. Soc., vol. 76, no. 12, pp. 2961-2970, December 1993.

- Kecskes, L. J., T. Kottke, and J. A. Puszynski. "Dynamic Consolidation of Combustion Synthesized  $\text{TiB}_2$ -TiC Ceramic Composites." Unpublished Work.
- Kecskes, L. J., R. F. Benck, and P. H. Netherwood, Jr. "Dynamic Compaction of Combustion Synthesized Hafnium Carbide." J. Am. Ceram. Soc., vol. 73, no. 2, pp. 383–387, February 1990.
- Kim, Y. W., and J. G. Lee. "Pressureless Sintering of Alumina-Titanium Carbide Composites." J. Am. Ceram. Soc., vol. 72, no. 8, pp. 1333–1337, August 1989.
- Kimura, I., N. Hotta, Y. Hiraoka, N. Saito, and Y. Yokota. "Sintering and Characterization of  $\text{Al}_2\text{O}_3$ - $\text{TiB}_2$  Composites." J. Eur. Ceram. Soc., vol. 5, no. 1, pp. 23–27, January 1989.
- Kny, E., and H. M. Ortner. "Aspects of Trace Elements in Hard Metals," Proceedings of the International Conference on the Science of Hard Materials, E. A. Almond, C. A. Brookes, and R. Warren (eds.), Adam Higler Ltd., Bristol, England, 1986.
- LaSalvia, J. C., L. W. Meyer, and M. A. Meyers. "Densification of Reaction-Synthesized Titanium Carbide by High-Velocity Forging." J. Am. Ceram. Soc., vol. 75, no. 3, pp. 592–602, March 1992.
- Logan, K. V. "Shaped Refractory Products and Method of Making Same." U.S. Patent 5,141,900, 1992.
- Logan, K. V., J. T. Sparrow, and W. J. S. McLemore. "Experimental Modeling of Particle-Particle Interactions During SHS of  $\text{TiB}_2$ - $\text{Al}_2\text{O}_3$ ." Combustion and Plasma-Synthesis of High-Temperature Materials, Z. A. Munir and J. B. Holt (eds.), pp. 219–228, New York: VCH Publishers, Inc., 1990.
- Logan, K. V., E. W. Price, and W. J. S. McLemore. "Differential Thermal Analysis of the  $\text{TiO}_2 + \text{B}_2\text{O}_3 + \text{Al}$  Thermite System/Development of an Experimental Model for Self-Propagating High Temperature Oxidation-Reduction Reactions." Materials Processing by Self-Propagating High-Temperature Synthesis (SHS), DARPA/ARMY SHS Symposium Proceedings, MTL SP 87-3, K. A. Gabriel, S. G. Wax, and J. W. McCauley (eds.), pp. 167–175, U.S. Government Printing Office, Washington DC, 1987.
- Materials Research Society. "Structure and Properties of Energetic Materials." Materials Research Society Symposium Proceedings, vol. 296, Pittsburgh, PA, 1993.
- Matsushita, J., S. Hayashi, and H. Saito. "Oxidation of  $\text{TiB}_2$ - $\text{Al}_2\text{O}_3$  Composites in Air." J. Ceram. Soc. Jpn., vol. 98, no. 3, pp. 308–310, March 1990.
- McCauley, J. W. "Historical and Technical Perspective on SHS." Cer. Eng. Sci. Proc., vol. 11, nos. 9–10, pt. 2, pp. 1137–1181, September–October 1990.

- Merzhanov, A. G. "Self-Propagating High-Temperature Synthesis: Twenty Years of Search and Findings." Combustion and Plasma Synthesis of High-Temperature Materials, Z. A. Munir and J. B. Holt (eds.), pp. 1-53, New York: VCH Publishers, Inc., 1990.
- Metals Powder Industries Federation. Particulate Materials and Process Advances in Powder Metallurgy. Vol. 9, Princeton, NJ, 1992.
- Misiolek, W. Z., T. S. Schurman, and N. D. Sopchak. "Studies of Pressure Assisted Reactive Sintering of TiC and TiB<sub>2</sub>." Particulate Materials and Process Advances in Powder Metallurgy, vol. 9, pp. 411-422, Metals Powder Industries Federation, Princeton, NJ, 1992.
- Miyamoto, Y., M. Koizumi, and O. Yamada. "High-Pressure Self-Combustion Sintering for Ceramics." J. Am. Ceram. Soc., vol. 67, no. 11, C224, November 1984.
- Munir, Z. A. "Synthesis of High-Temperature Materials by Self-Propagating Combustion Methods." Cer. Bull., vol. 67, no. 2, pp. 342-349, February 1988.
- Munir, Z. A., and J. B. Holt. "Combustion and Plasma Synthesis of High-Temperature Materials." Z. A. Munir and J. B. Holt (eds.), New York: VCH Publishers, Inc., 1990.
- Munir Z. A., and U. Anselmi-Tamburini. "Self-Propagating Exothermic Reactions: The Synthesis of High-Temperature Materials by Combustion." Mater. Sci. Rep., vol. 3, nos. 7-8, pp. 277-365, May 1989.
- Niiler, A., L. J. Kecskes, and T. Kottke. "Shock Consolidation of Combustion Synthesized Ceramics." Combustion and Plasma-Synthesis of High-Temperature Materials, Z. A. Munir and J. B. Holt (eds.), pp. 309-314, New York: VCH Publishers, Inc., 1990.
- Niiler, A., L. J. Kecskes, T. Kottke, P. H. Netherwood, Jr., and R. F. Benck. "Explosive Consolidation of Combustion Synthesized Ceramics: TiC and TiB<sub>2</sub>." BRL-TR-2951, U.S. Army Ballistic Research Laboratory, Aberdeen Proving Ground, MD, 1988.
- Nishida, T., N. Miyazaki, H. Saito, and K. Urabe. "High Pressure Hot-Pressing of TiC and TiC-Al<sub>2</sub>O<sub>3</sub> Utilizing the Heat of Self Combustion." J. Jpn. Soc. of Powder and Powd. Metall., vol. 40, no. 1, pp. 24-28, January 1993.
- Rabin, B. H., G. E. Korth, and R. L. Williamson. "Fabrication of Titanium Carbide-Alumina Composites by Combustion Synthesis and Subsequent Dynamic Consolidation." J. Am. Ceram. Soc., vol. 73, no. 7, pp. 2156-2157, July 1990.
- Rice, R. W., W. J. McDonough, G. Y. Richardson, J. M. Kunetz, and T. Schroeter. "Hot Rolling of Ceramics Using Self-Propagating High-Temperature Synthesis." Ceram. Eng. Sci. Proc., vol. 7, nos. 5-6, pp. 751-60, May-June 1986.

- Stadlbauer, W., W. Kladnig, and G. Gritzner. "Al<sub>2</sub>O<sub>3</sub>-TiB<sub>2</sub> Composite Ceramics." J. Mater. Sci. Lett., vol. 8, no. 10, pp. 1217-1220, October 1989.
- Tampieri, A., E. Landi, and A. Bellosi. "On the Oxidation Behavior of Monolithic TiB<sub>2</sub> and Al<sub>2</sub>O<sub>3</sub>-TiB<sub>2</sub> and Si<sub>3</sub>N<sub>4</sub>-TiB<sub>2</sub> Composites." J. Thermal Anal., vol. 38, no. 12, pp. 2657-2668, December 1992.
- TMS. TMS Annual Meeting on Reaction Synthesis of Materials. Met. Trans. A, vol. 23A, no. 1, pt. 1, TMS, Warrendale, PA, 1992.
- Vecchio, K. S., J. C. LaSalvia, M. A. Meyers, L. W. Meyer, and G. T. Gray. "Microstructural Characterization of Self-Propagating High Temperature Synthesis/Dynamically Compacted and Hot-Pressed Titanium Carbides." Met. Trans. A, vol. 23A, no. 1, pt. 1, pp. 87-97, January 1992.
- Vershinnikov, V. I., S. S. Mamyan, and G. Georgiev. "Regularities of the Synthesis of Composite Ceramic Powder TiB<sub>2</sub>-Al<sub>2</sub>O<sub>3</sub> and a Material on Its Base." Inzhenerno-Fizicheskii Zhurnal, vol. 65, no. 4, pp. 496-500, October 1993.
- Wang, L., M. R. Wixom, and L. J. Thompson. "Structural and Mechanical Properties of TiB<sub>2</sub> and TiC Prepared by Self-Propagating High Temperature Synthesis/Dynamic Compaction." J. Mat. Sci., vol. 29, no. 2, pp. 534-543, January 1994.
- Yamada, O., Y. Miyamoto, and M. Koizumi. "High-Pressure Self-Combustion Sintering of Titanium Carbide." J. Am. Ceram. Soc., vol. 70, no. 9, C206-C208, September 1987.

<u>NO. OF COPIES</u>	<u>ORGANIZATION</u>
2	DEFENSE TECHNICAL INFO CTR ATTN DTIC DDA 8725 JOHN J KINGMAN RD STE 0944 FT BELVOIR VA 22060-6218

1	DIRECTOR US ARMY RESEARCH LAB ATTN AMSRL OP SD TA 2800 POWDER MILL RD ADELPHI MD 20783-1145
---	---

3	DIRECTOR US ARMY RESEARCH LAB ATTN AMSRL OP SD TL 2800 POWDER MILL RD ADELPHI MD 20783-1145
---	---

1	DIRECTOR US ARMY RESEARCH LAB ATTN AMSRL OP SD TP 2800 POWDER MILL RD ADELPHI MD 20783-1145
---	---

ABERDEEN PROVING GROUND

5	DIR USARL ATTN AMSRL OP AP L (305)
---	---------------------------------------

<u>NO. OF COPIES</u>	<u>ORGANIZATION</u>	<u>NO. OF COPIES</u>	<u>ORGANIZATION</u>
1	HQDA ATTN SARD TR WASHINGTON DC 20301	1	CALIFORNIA INST OF TCHNLGY ATTN DR T VREELAND KECK LABS MS138 78 PASADENA CA 91125
4	COMMANDER US ARMY RESEARCH OFC ATTN DR I AHMAD DR E CHEN DR A CROWSON DR R REEBER PO BOX 12211 RESEARCH TRIANGLE PARK NC 27709-2211	1	CERACON INC ATTN DR R RAMAN 1101 N MARKET BLVD STE 9 SACRAMENTO CA 95834
1	DIRECTOR BENET LABORATORIES ATTN AMSTA AR CCB DR W KITCHENS JR WATERVLIET NY 12189	1	CERAMATEC INC ATTN DR R CUTLER 2425 S 900 WEST SALT LAKE CITY UT 84119
1	COMMANDER USA AMCCOM ATTN SMCAR ESP L ROCK ISLAND IL 61299	2	GENERAL SCIENCES INC ATTN DR P ZAVITSANOS DR J GEBHARDT PO BOX 185 PLYMOUTH MEETING PA 19462
2	COMMANDER USA FOREIGN SCI & TECH CTR ATTN MR J CRIDER MR W MARLEY 220 SEVENTH ST NE CHARLOTTESVILLE VA 22901	4	GEORGIA INST OF TCHNLGY ATTN DR K LOGAN DR N THADHANI MR G VILLALOBOS DR J WALTON 778 ATLANTIC DR ATLANTA GA 30332
1	COMMANDER ARPA ATTN DR P PARRISH 3701 N FAIRFAX DR ARLINGTON VA 22203-1714	3	IDAHO NATL ENGNRNG LAB ATTN DR B RABIN DR G KORTH DR R WRIGHT PO BOX 1625 IDAHO FALLS ID 83415
1	AIRTRON DIVISION ATTN DR J INGS 200 E HANOVER AVE MORRIS PLANES NJ 07950	2	DIRECTOR LAWRENCE LIVERMORE NATL LAB ATTN DR J HOLT L369 DR D MAIDEN MSL71 PO BOX 808 LIVERMORE CA 94550
1	ALCOA LABORATORIES ALCOA TECHNICAL CENTER ATTN DR A BECKER ALCOA CENTER PA 15069	1	LOCKHEED PALO ALTO RSRCH LAB ATTN DR A HARDT 3251 HANOVER ST PALO ALTO CA 94304
1	BATTELLE ATTN MR V LINSE 505 KING AVE COLUMBUS OH 43201		

NO. OF COPIES	ORGANIZATION
5	DIRECTOR LOS ALAMOS NATL LAB ATTN DR R BEHRENS MS3C348 DR K WYLIE MSG780 DR D SANDSTROM MSG756 DR S CALDWELL DR R FRANZ MSD466 LOS ALAMOS NM 87545
3	MARTIN MARIETTA LABS ATTN DR D NAGLE DR S WINZER MR M RILEY 1450 S ROLLING RD BALTIMORE MD 21227
1	NATL BUREAU OF STANDARDS ATTN DR S J SCHNEIDER RM A257 BLDG 223 WASHINGTON DC 20234
3	NEW MEXICO INST OF MINING & TECH CTR FOR EXPLSVE TECH & RSRCH ATTN DR A MILLER DR P PERSSON MR V JOSHI SOCORRO NM 87801
1	NEW MEXICO INST OF MINING & TECH MATRLS & METALLURGICAL ENGRNG ATTN DR O INAL SOCORRO NM 87801
1	DIRECTOR SANDIA NATIONAL LABS ATTN DR S MARGOLIS COMBUSTION RESEARCH FACILITY LIVERMORE CA 94550
1	SOUTH DAKOTA SCHL OF MINES & TECH CHEMSTRY & CHEMCL ENGRG DEPT ATTN DR J PUSZYNSKI 501 E ST JOSEPH ST RAPID CITY SD 57701
1	STATE UNIV OF NEW YORK DEPT OF CHEMICAL ENGRG ATTN DR V HLAVACEK AMHERST NY 14260

NO. OF COPIES	ORGANIZATION
1	UNIV OF CALIFORNIA COLLEGE OF ENGINEERING ATTN DR Z MUNIR DAVIS CA 95616
2	UNIV OF CALIFORNIA SAN DIEGO INST OF MCHNCS OF MTRLs ATTN DR M MEYERS DR J LASALVIA 9500 GILMAN DR LA JOLLA CA 92093
	<u>ABERDEEN PROVING GROUND</u>
34	DIR, USARL ATTN: AMSRL-WT, D. ECCLESHALL G. KLEM AMSRL-WT-W, C. MURPHY AMSRL-WT-WA, H. ROGERS AMSRL-WT-WB, W. DAMICO AMSRL-WT-WC, J. ROCCHIO AMSRL-WT-WD, P. BERNING D. DANIEL A. GAUSS, JR. C. HOLLANDSWORTH L. KECSKES (6 CPS) T. KOTTKE A. NILER F. PIERCE G. THOMSON AMSRL-WT-TA, R. BENCK W. BRUCHEY W. GILLICH W. GOOCH G. HAUVER T. HAVEL E. HORWATH AMSRL-WT-TA, D. MACKENZIE P. NETHERWOOD, JR. AMSRL-WT-TC, E. KENNEDY AMSRL-WT-TD, A. DIETRICH, JR. T. FARRAND K. FRANK P. KINGMAN

NO. OF  
COPIES ORGANIZATION

ABERDEEN PROVING GROUND (CONT.)

4 DIR USARL (CR)  
ATTN: AMSRL MA C  
DR D VIECHNICKI  
AMSRL MA CC  
DR R ADLER  
DR J WELLS  
AMSRL MA CA  
DR M STAKER

NO. OF  
COPIES ORGANIZATION

- 1 GOVT INDUSTRIAL RESEARCH INSTITUTE  
ATTN DR N SATA  
4 5 1 NIGATAKE  
MIYAGINO KU  
SENDAI MIYAGI 983 JAPAN
- 1 NATIONAL RESEARCH INSTITUTE FOR METALS  
ATTN DR Y KAIEDA  
2 3 12 NAKAMEGURO  
MEGURO KU  
TOKYO 153 JAPAN
- 1 OSAKA UNIVERSITY  
ATTN DR Y MIYAMOTO  
IBARAKI  
OSAKA 567 JAPAN
- 1 RYUKOKU UNIVERSITY  
ATTN DR M KOIZUMI  
1 5 YOKOYA  
OE CHO  
OTSU SHIGA 520 21 JAPAN
- 2 TOKYO INSTITUTE OF TECHNOLOGY  
ATTN DR A SAWAOKA  
DR O ODAWARA  
4259 NAGATSUATA  
MIDORI KU  
YOKOHAMA 227 JAPAN

INTENTIONALLY LEFT BLANK.

## USER EVALUATION SHEET/CHANGE OF ADDRESS

This Laboratory undertakes a continuing effort to improve the quality of the reports it publishes. Your comments/answers to the items/questions below will aid us in our efforts.

1. ARL Report Number ARL-TR-918 Date of Report December 1995
2. Date Report Received \_\_\_\_\_
3. Does this report satisfy a need? (Comment on purpose, related project, or other area of interest for which the report will be used.) \_\_\_\_\_  
\_\_\_\_\_  
\_\_\_\_\_
4. Specifically, how is the report being used? (Information source, design data, procedure, source of ideas, etc.) \_\_\_\_\_  
\_\_\_\_\_  
\_\_\_\_\_
5. Has the information in this report led to any quantitative savings as far as man-hours or dollars saved, operating costs avoided, or efficiencies achieved, etc? If so, please elaborate. \_\_\_\_\_  
\_\_\_\_\_  
\_\_\_\_\_
6. General Comments. What do you think should be changed to improve future reports? (Indicate changes to organization, technical content, format, etc.) \_\_\_\_\_  
\_\_\_\_\_  
\_\_\_\_\_  
\_\_\_\_\_

CURRENT  
ADDRESS

\_\_\_\_\_  
Organization

\_\_\_\_\_  
Name

\_\_\_\_\_  
Street or P.O. Box No.

\_\_\_\_\_  
City, State, Zip Code

7. If indicating a Change of Address or Address Correction, please provide the Current or Correct address above and the Old or Incorrect address below.

OLD  
ADDRESS

\_\_\_\_\_  
Organization

\_\_\_\_\_  
Name

\_\_\_\_\_  
Street or P.O. Box No.

\_\_\_\_\_  
City, State, Zip Code

(Remove this sheet, fold as indicated, tape closed, and mail.)  
(DO NOT STAPLE)